Preparation and Luminescent Performances of Tellurite Glass Coated $CsPbBr_3$@glass Film for Remote LED Color Converter

Huanhuan Zhang[1], Jialing Ou[1], Guoying Zhao[1*], Jingshan Hou[1], Yufeng Liu[1], Xin Qiao[2], Zhongzhi Wang[2], Ji-Guang Li[3], Yongzheng Fang[1*]

[1] *School of Materials Science and Engineering, Shanghai Institute of Technology, Shanghai 201418, PR China*

[2]*Baotou Research Institute of Rare Earths, Baotou, 014030, China*

[3]*Research Center for Functional Materials, National Institute for Materials Science, Tsukuba, Ibaraki 305-0044, Japan*

[*]*Corresponding author, E-mail addresses: zhaogy135@126.com; fyz1003@sina.com.*

ABSTRACT: We know that perovskite quantum dot (PQD) glass is one of the effective ways to achieve high stability, high reliability and high weather resistance. However, quantum dot glass is still unable to achieve completely uniform crystallization as a whole, so quantum dot glass has to be used in the form of powder by mixing glue. The use of organic matter leads to the problems of heat accumulation and stability. In this work, the concept of double cladding encapsulation was realized to solve the above problems in the application of quantum dot glass, and the remote inorganic fluorescent film is prepared. $CsPbBr_3$ PQDs embedded in borosilicate glass (PQDs@glass) were prepared using traditional melting-quenching and heat-treatment processes. By optimizing the raw material composition and melting conditions, excellent PQDs@glass were obtained, and its photoluminescence quantum yield (PLQY) was as high as 88.06%. The $CsPbBr_3$ PQDs embedded borosilicate glass has been dispersed in tellurite glass film again along with color-compensatory red-emitting nitride phosphor, which is a doubly encapsulated system with inorganic glass matrixes to improve stability and color-tunability. A series of prototypes light-emitting diode devices were assembled based on the as-made doubly encapsulated glass film with a commercial blue chip, resulting in bright white light luminescence at a color temperature of 3920 K and a high color rendering index of 87.2.

Keywords: Remote glass film; $CsPbBr_3$ perovskite quantum dot; High quantum yield; Double

Encapsulation

1. Introduction

Recently, due to the unique optical properties, inorganic cesium lead halide ($CsPbX_3$, X = Cl, Br, I) perovskite quantum dots (PQDs) have attracted growing attention[1-4]. The photoluminescence (PL) of lead halide perovskite PQDs covers the entire visible spectral region with high quantum yield, which may find potential applications in various photoelectronic devices[5-8]. Thermal corrosion of monodisperse perovskite $CsPbBr_3$ nanostructures in amorphous glass substrates and during co-sintering with low melting point glass is negligible, ensuring good luminous properties. By the passivation of surface traps in wet-chemical synthesis strategy, the photoluminescence quantum yields (PLQYs) of $CsPbBr_3$ can reach over 90% in green spectral region[9]. However, the PLQYs of glass-stabilized $CsPbBr_3$ is relatively lower than the colloidal counterpart, and the highest value of PLQY is 81% that is obtained from boron-germanium glass, which hampers their practical application for photoelectronic devices[10]. In general, borosilicate glass is characterized by excellent physical and chemical stability compared to other glass systems when exposed to air or moisture. Owning to the ligand sensibility of $CsPbBr_3$ PQDs in glass, it is necessary to optimize the borosilicate glass grid structure to achieve high PLQY and long-term stability.

As is known to all, the present commercial w-LED is assembled with yellow yttrium aluminum garnet phosphor and packaging material-organic epoxy silicone mixed, using "dispensing" technology means coated on LED chip[11-14]. However, as the LED power increases, the operating time increases, resulting in the PN junction temperature rise, at this time the chip temperature can be as high as 150~200 °C, which will make the phosphor temperature quenching effect[15,16]. It will also make LED device efficiency decline, color coordinate deviation, service life suddenly reduced service life of a sudden reduction[17,18]. It has been proposed to replace organic materials such as phosphorus in glass (PiG) with inorganic components. The PiG method is a simple mixture of transparent glass and phosphor sintered together at a certain temperature. Yoon et al. suggested a novel inorganic color converter for white LED with a single phosphor-in-glass (PiG) plate. $CsPbBr_3$ perovskite nanocrystals embedded in germanate glass was used as a green phosphor and mixed with a transparent silicate glass to prepare the PiG plate. The photo stability and thermal stability of $CsPbBr_3$ perovskite nanocrystals are improve[19]. Compared to glass ceramic plate, PiG film can be

easily sintered and its color coordination can be simply controlled by adjusting the rations of PQDs@glass and phosphors. In addition, PiG film has high thermal conductivity and adjustable high refractive index, which can diffuse the heat accumulated on the phosphorus layer onto the silicon glass substrate. Therefore, the PiG film exhibits the robust stability when compared with the organic encapsulants. Red nitride phosphors have been widely studied for their excellent photoluminescent behaviors. Unfortunately, the commercial red nitride phosphors suffer from the poor structural stability during the low temperature co-sintering procedure[20]. Therefore, the mother glass protecting the embedded phosphor particles is a key factor identifying the photoluminescent performances of PiG.

Tellurite glass is characterized by TeO_2 as the main component, often by adding some oxides and halides to improve the glass forming ability and stability[21]. As a kind of heavy metal oxide glasses, tellurite glass has its own unique advantages including: high refractive index (around 2.0), wide infrared transmission range (0.35-5 um), low phonon energy in oxide glass (about 600-850 cm^{-1}) and low melting temperature (800-950 °C)[22]. Benefiting from the high refractive index and low phonon energy, high absorption and emission cross section and low non-radiative transition rates of rare earth ion can be obtained[23,24]. As to the use of mother glass for PiG, the high refractive index of tellurite glass is favorable to matching the refractive index of doped phosphor to a greater extent[25]. Besides, the relatively low glass transition temperature will reduce the thermal corrosion of photoluminescent phase. Therefore, tellurite glass is considered to be an excellent candidate for PiG.

In this study, the concept of double cladding encapsulation was realized in borosilicate stabilized $CsPbBr_3$ PQDs using tellurite glass as the outer clad. Firstly, we obtain the $CsPbBr_3$ PQDs with the high quantum efficiency through the regulation of glass grid. By spinning coating technology, the as-made borosilicate stabilized $CsPbBr_3$ PQDs and commercial nitride phosphors are uniformly dispersed in tellurite glass on the silica substrate. Finally, after determining the optimal sintering temperature, we prepared a series of QiG(quantum dots in glass)@glass flakes and then mounted them on a blue chip with a wavelength of 450 nm to produce white light. The effects of sintering temperature and glass-phosphor ratio on the properties of QiG@glass were discussed.

2. Experimental section

2.1 Fabrication of $CsPbBr_3$ PQDs in borosilicate glasses

The glass carrier is prepared from high-purity SiO_2, H_3BO_3 and ZnO powders, and the perovskite components were added into Cs_2CO_3, $PbBr_2$ and KBr (CPB). The purity and supplier of all reagents are given in Table 2. All experiments are conducted without toxic and harmful organic reagents. All raw materials are first ground into a powder in an agate mortar and then transferred to a corundum crucible. The powder is melted in a muffle furnace at 1200 °C for 15 min. The molten glass is then poured into a preheated copper mold and immediately transferred to a muffle furnace at 350 °C and held for 2 h to release stress. Finally, the precursor glass was heat treated near the glass transition temperature to obtain $CsPbBr_3$ PQDs multi-component glass. Stored at a heat treatment temperature of 470 °C for 10 hours, a series of $CsPbBr_3$ PQDs multi-component glass samples were obtained. For further study, the resulting glass is ground into a powder or optically polished.

Table 1. Glass compositions [$xSiO_2$- (67-x) B_2O_3-16ZnO (x=35, 38, 41, 48, 58 mol%)] and the added perovskite-related components.

Sample	SiO_2	B_2O_3	ZnO	Cs_2CO_3	$PbBr_2$	KBr
35Si	35	32	16	9	3	6
38Si	38	29	16	9	3	6
41Si	41	26	16	9	3	6
48Si	48	19	16	9	3	6
58Si	58	9	16	9	3	6
8CPB	38	29	16	8	2	4
9CPB	38	29	16	9	3	6
10CPB	38	29	16	10	4	8
11CPB	38	29	16	11	5	10
12CPB	38	29	16	12	6	12
9CPB-1.8	38	29	16	9	5.4	10.8
9CPB-2.1	38	29	16	9	6.3	12.6
9CPB-2.4	38	29	16	9	7.2	14.4
9CPB-2.7	38	29	16	9	8.1	16.2
9CPB-3.0	38	29	16	9	9	18

2.2 Fabrication of QiG@glass films

Glasses with composition $20B_2O_3$-$60TeO_2$-10ZnO-$10Na_2O$ were prepared by using analytical grade B_2O_3, TeO_2, ZnO, Na_2CO_3 as starting materials. Based on a certain stoichiometric ratio, the starting materials were weighted and mixed together. It was thoroughly ground and placed in an

alumina crucible and then melted for 0.5 h at 950 °C in a muffle furnace. Subsequently, the melt were poured into a preheated brass mold and annealed at 300 °C for 15 h. Glass samples were cut and carefully polished to meet optical measurements. Each sample looks more transparent.

The slurries were mixed by suitable powder dosing: the prepared glass-stabilized $CsPbBr_3$ PQDs powder, $Sr_2Si_5N_8$ red phosphor, and tellurite glass matrix. All powders were mixed into organic vehicle which composition were terpilenol and ethyl cellulose at 80 K for 12 h by 700 rpm. The mixed slurry is spin coated onto the glass substrate (r_Φ = 20 mm) by scraping and then the resultant samples were dried at 150 °C for 5 h in order to make the organic matter completely volatile. Finally, QiG@glass film was obtained by sintering the glass film at 460 °C for 30 min.

Table 2. Purity and supplier of each starting reagent.

Start reagent	Purity	Supplier
SiO_2	GR	Shanghai Maclin Biochemical Technology Co., LTD
H_3BO_3	GR	Shanghai Titan Technology Co., LTD
ZnO	AR, 99.0%	Shanghai Titan Technology Co., LTD
Cs_2CO_3	99.9%	Shanghai Merrier Chemical Technology Co., LTD
KBr	AR, 99.0%	Sinopharm Chemical Reagent Co. LTD
$PbBr_2$	99 %	Shanghai Titan Technology Co., LTD
TeO_2	99.99%	Chengdu Zhongjian Materials Optoelectronic Materials Co., LTD
Na_2CO_3	AR, ≥ 99.8%	Shanghai Titan Technology Co., LTD

2.3 Characterization

The phase purity of phosphor powders and QiG@glass firms was confirmed by using an X-ray powder diffractometer (TD-3500, Dandong, China) with Cu Kα irradiation at 40 kV and 40 mA. The microstructure and elemental mappings were observed by a field-emission scanning microscope (SU70, Hitachi) equipped with an energy-dispersive X-ray spectroscope (EDS) system and Transmission Electron Microscopy (FEI Tecnai F20). The photo-luminescence (PL) and photo-luminescence excitation (PLE) of the samples were measured using a spectrometer (Hitachi F-7000) with a xenon discharge lamp. FS5 fluorescence spectrometer is standard equipped with absorption detector, which can achieve fluorescence and UV testing functions on the same instrument at the same time, so we tested the quantum yield by FS5. Decimal methods can also be applied to a wider

range of sample types and are the only reliable method for samples such as solid powder and thin films. The test requires an integrating sphere that is coupled to the fluorescence spectrometer as a test attachment. In absolute quantum yield testing, all light emitted by a sample is captured using an integrating sphere, and the quantum yield is determined by comparing the number of photons emitted to the number of photons absorbed. Such as formula (1):

$$\eta = \frac{number\ of\ photons\ emitted}{number\ of\ photons\ absorbed} \tag{1}$$

The difference in integral area between the sample and the reference indicates the number of the absorbed photons. The emitted photons were determined by integrating the related emission band. Test the blank curve with the blank sample that comes with the integrating sphere. The scattering curve and the sample curve are combined to calculate the quantum yield. The optical properties of the w-LED module are obtained in the integrating sphere, including chromaticity color coordinates, correlated color temperature (CCT), color rendering index (CRI), luminous efficiency, and electroluminescence (EL) emission spectroscopy (HAAS-2000).

3. Results and Discussion

3.1 Microstructure and luminescence of PQDs@glass

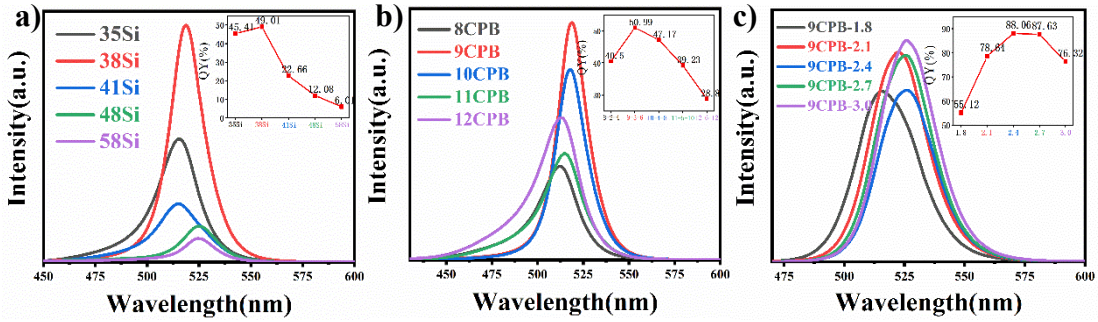

Fig. 1 (a-c) Photoluminescence spectra and PLQY of $xSiO_2$- (67-x) B_2O_3-16ZnO (x=35, 38, 41, 48, 58 mol%) glass with different CPB components excited at 365 nm.

Fig. 1 shows the photoluminescence (PL) spectra and PLQYs of $CsPbBr_3$ PQDs from borosilicate samples under excitation at 365 nm and 450 nm. It can be seen that the well crystallized $CsPbBr_3$ PQDs formed in B39Si28 glass containing 9CPB-2.4 has the highest PLQY value (88.06%). With the decrease of B/Si ratio, the emission intensity increases first and then decreases, reaching the maximum value at Si38B29, and the change of quantum yield also presents the similar trend. The photoluminescence of sample exhibits the narrow-band emission characteristics of

quantum dot materials. It can be seen from Fig. 1(a) that the luminescence of $CsPbBr_3$ PQDs doped glass is controlled by changing the topological structure of the glass. The glass grid structure has an important impact on the precipitation and growth of quantum dots from mother glass, which in turn affects the luminescence performance. Based on our previous work, there exists an optimal B/Si molar ratio that possesses the moderate glass rigidity, which can boost the precipitation of CPB elements and accelerate the growth of nanocrystals from glass network[26]. Therefore, Si38B29 sample is selected as glass host to optimize CPB concentration (PL spectra shown in Fig. 1(b and c))[27]. In order to compensate for the volatile loss of Br element during the melting procedure, excess amounts of halogen compounds, $PbBr_2$ and KBr, needed to be added to the raw material. With the increase of doped concentration, more and more quantum dots polymerize and grow in glass, resulting in an increase in PQDs concentration, it is worth noting that a moderate excess of Br supplementation in raw materials is more conducive to the growth of PQD in glass. The results show that the quantum efficiency of the sample reaches the maximum when the CPB concentration is further increased to $9Cs_2CO_3$−$7.2PbBr_2$−14.4KBr mol%.

As showed in TEM image (shown in Fig. 2(a)), the $CsPbBr_3$ PQDs are evenly dispersed in the glass matrix, and their average particle size is 2.98 nm. High-resolution TEM (HRTEM) image (Fig. 2(b)) evidences homogeneous precipitation of $CsPbBr_3$ PQDs with well-resolved lattice fringes with high-crystallinity, which shows clear lattice fringes with an interplanar distance of 0.288 nm. The lattice fringes have 0.288 nm interplanar distance that corresponds to the [200] lattice plane of the cubic $CsPbBr_3$[28,29]. It can be seen that the PQDs in the glass are different from the cubic form of the colloidal PQDs prepared by wet chemistry, and the PQDs in the glass is a spherical form, which may be due to the restriction effect of inorganic oxidized glass on the growth of PQDs. Elemental mapping of these nanocrystals suggested that these nanocrystals were highly rich in Cs, Pb and Br. In general, the precipitation of $CsPbBr_3$ nanocrystals in the sample was confirmed.

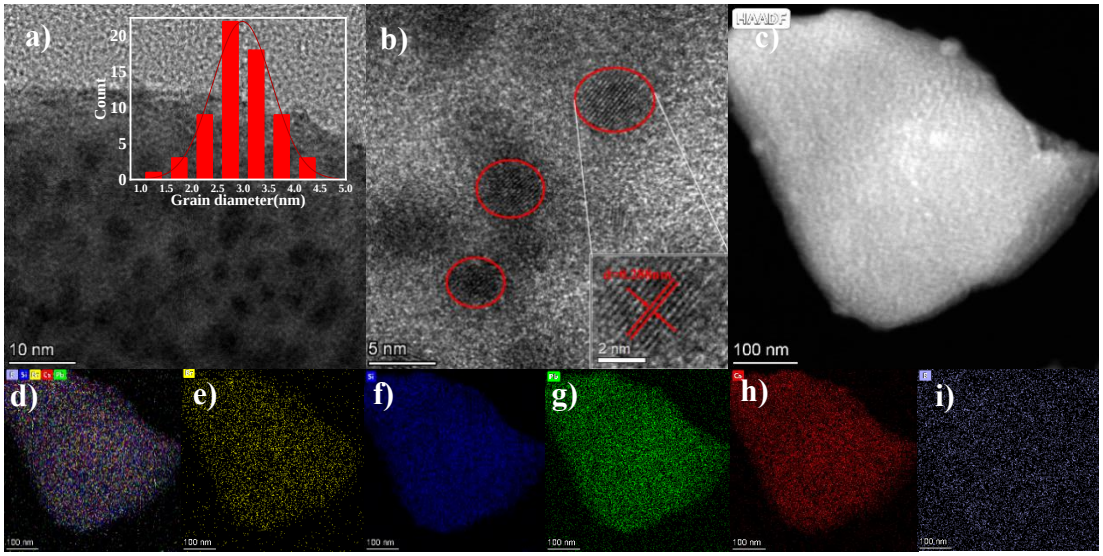

Fig. 2 (a and b) TEM image of the $CsPbBr_3$ PQDs@glass. (c) HRTEM micrograph of the $CsPbBr_3$ PQDs@glass. (d-i) B, Si, Cs, Pb, and Br elemental mappings.

3.2. Microstructure and luminescence of QiG@glass film.

QiG@glass films have high thermal stability compared to conventional organic encapsulation; Good moisture resistance; It has the characteristics of corrosion resistance and high chemical stability. The XRD patterns of quantum dot glass, red phosphor and QiG@glass samples are shown in Fig. 3(a). The different peaks correspond to the $Sr_2Si_5N_8$ and PQDs, which is in accord with that of the pure $Sr_2Si_5N_8$ phosphor and standard card of $CsPbBr_3$ (PDF #75–0412), respectively. The QiG@glass film has little effect on the phosphors, and the fluorescent crystal phase is intact in glass matrix. Furthermore, the 9CPB-2.4 QiG@glass film was chosen to check the possible reaction between as-prepared glass and the phosphor, SEM, EDS and EDS mapping were carried out. Fig. 3(b-h) indicates that the glass and phosphor powder are uniformly distributed in the tellurite glass matrix. The moderate concentration of pores in film is beneficial to reducing the reflection of incident light to improve the utility of pump light [30,31]. The cross section image (shown in Fig. 3(c)) suggests the phosphor layer with a thickness of approximately 24.54μm has been well adhered on the surface of silica glass substrate after sintering.

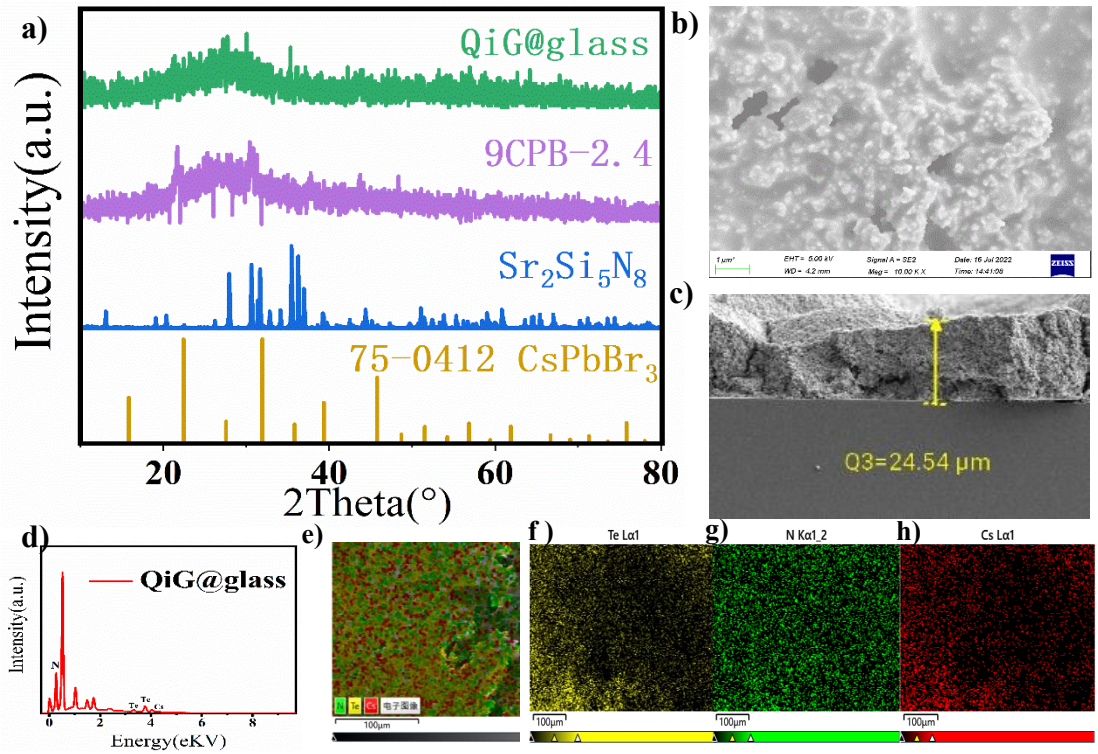

Fig. 3 (a) The XRD patterns of quantum dot glass, red phosphor and QiG@glass samples. (b and c) SEM of QiG@glass film. (d) EDS spectrum of QiG@glass film. (e-h) Mapping image of Te, N and Cs.

We prepared a series of W-LEDs by changing the ratio of quantum dot glass powder to red phosphor. To research the luminescence properties, the prepared QiG@glass film is assembled on the top of the blue chip under the 450 nm irradiation with a drive current of 10 mA (Fig. 4 (b)). To produce white light, we mixed the red phosphor $Sr_2Si_5N_8$ with glass powder at the content sub-point and then embedded in the tellurite glass to form a QiG@glass. The weight ratio of glass to phosphorus is adjusted from 10:1 to 14:1. The resulting electroluminescence diagram and color coordinates are shown in Fig. 4(a and c). According to EL spectrum and chromaticity diagram, the ratio of glass to phosphor is 13:1, which is the best ratio to produce white light. As the proportion of glass powder in QiG@glass increased, the 450 nm blue component in the spectrum increased, and the light color changed from warm white to cold white, as shown in Fig. 4(c).

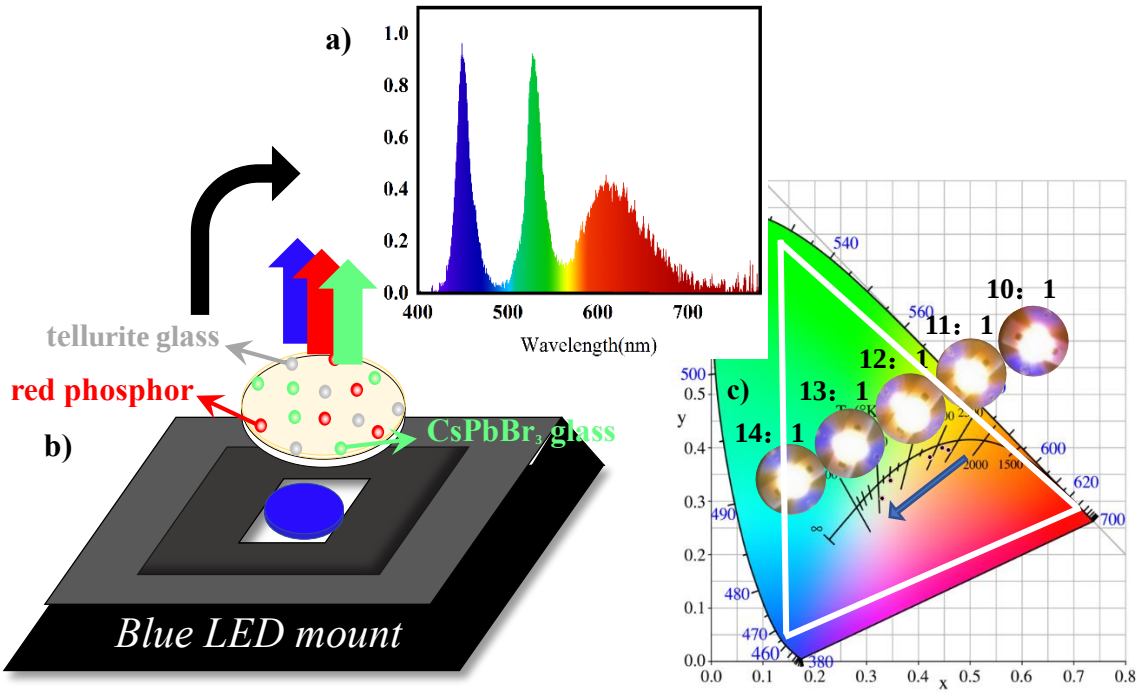

Fig. 4 (a) Optimum ratio electroluminescence diagram. (b) Schematic diagram of LED package. (c) Color coordinates at different scales and real pictures.

Fig. 5(a) shows the excitation and emission spectra of the glass powder and phosphor used in the experiment, respectively. It can be seen that the emission peak of the glass powder is located at 526 nm. It indicates that the emission spectrum of the glass powder and the excitation spectrum of the red powder have a large area of spectral overlap. The emission spectrum of glass powder can theoretically be reabsorbed by red powder and converted into red emission spectrum, which improves the emission intensity of red light, and correspondingly reduces the probability of green light transmitted out of the film to the space. QiG@glass films (the ratio of glass to red phosphor power was 13:1) were prepared at a sintering temperature of 460 °C to 490 °C. As the sintering temperature increased, the color of the sample gradually darkened, and the color rendering index decreased from 87.2 to 55.7. The color temperature increased from 3920 K to 12821 K. The results show that the sintering conditions of the QiG@glass film have a significant effect on the performance of the red phosphor. This may be due to the instability of the crystal phase structure of nitride in glass[32-37]. At a low sintering temperature of 460 °C, the thermal damage can be reduced for better luminous performance. At this temperature, warm white light with high visibility can be obtained.

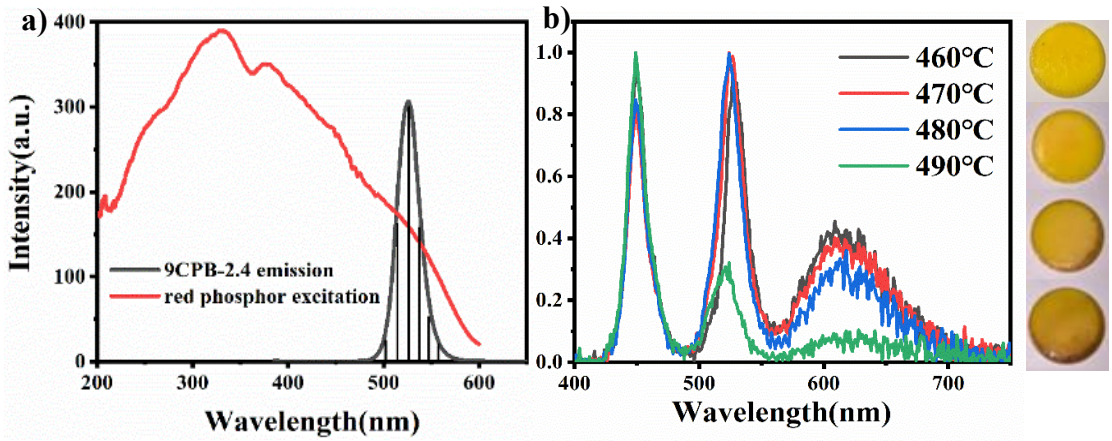

Fig. 5 (a) Emission spectrum of glass powder and excitation spectrum of phosphor powder. (b) The electroluminescence diagram of QiG@glass at different sintering temperatures.

3.3 The stability of QiG@glass film

The stability of QiG@glass is an important parameter for its applications. The PL temperature dependence was investigated (Fig. 6(a)), showing the PL spectra of QiG@glass at eight typical temperatures of 25, 50, 75, 100, 125, 150, 175 and 200 °C (298-473 K). With increasing of temperature (solid lines), the PL intensity decreased and its peak wavelength was blue-shifted. When the sample were cooled (dashed lines), the PL intensity and the shifted peak wavelength were reversibly recovered. These characteristic temperature dependent PL intensity change and emission peak shift have been commonly found in $CsPbBr_3$ perovskite nanocrystals, which can be attributed to the thermal expansion and phonon−electron interaction[19]. Furthermore, the long-term stability for the QiG@glass samples was investigated by dipping them in water. PL spectra shows that there is no obvious change of PL intensity (Fig. 6(c)) in water for 60 days. Under the protection of tellurite glass and borosilicate glass, the emission intensity is basically unchanged after 60 days of immersion in water. This result confirms that tellurite glass carriers and borosilicate glass are indeed effective in protecting PQDs from decomposition.

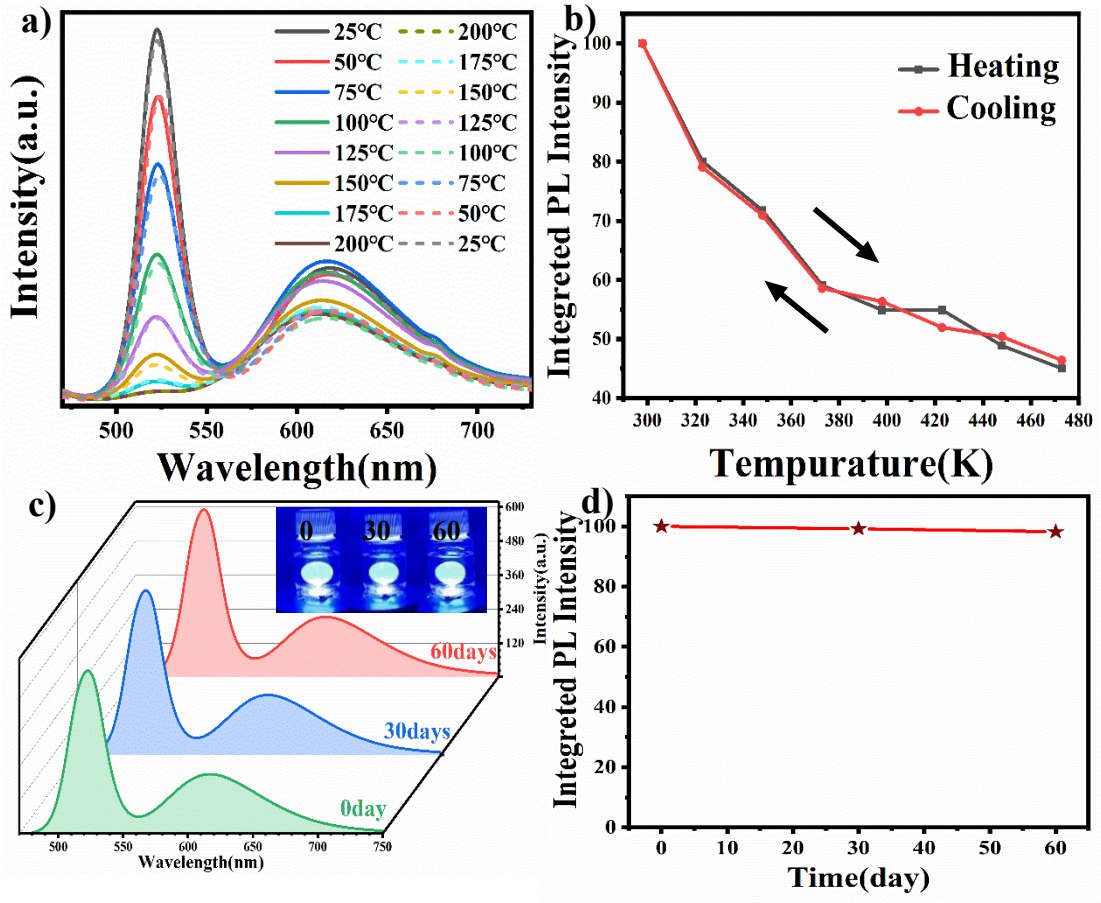

Fig. 6 (a) Temperature-dependent PL spectra (λ_{ex} = 450 nm) for the QiG@glass in the temperature range of 298-473 K. (b) Integral photoluminescence intensities of QiG@glass specimens recorded during thermal cycling experiment. (c) PL spectra for QiG@glass directly immersing in water for 60 days and inset is a photo of glass in water under the illumination of a blue light chip. (d) Integrated photoluminescence intensities in water stability.

The QIG@glass film was irradiated with a blue light of 300 mA forward current for 0, 3, 9, 21, 45, 93 h, equally its luminescence spectrum was tested (Fig. 7(a and b)), and the luminous intensity only decreased by about 3%. By introducing oxygen into the tube furnace, the oxygen stability of the film was studied by making the film stand in the oxygen environment for 0, 12, 48, 96 h. The luminescence spectrum shows (Fig. 7(c and d)) with no significant change in luminous intensity. Therefore, tellurite glass matrix can protect the stability of PQDs and phosphors effectively.

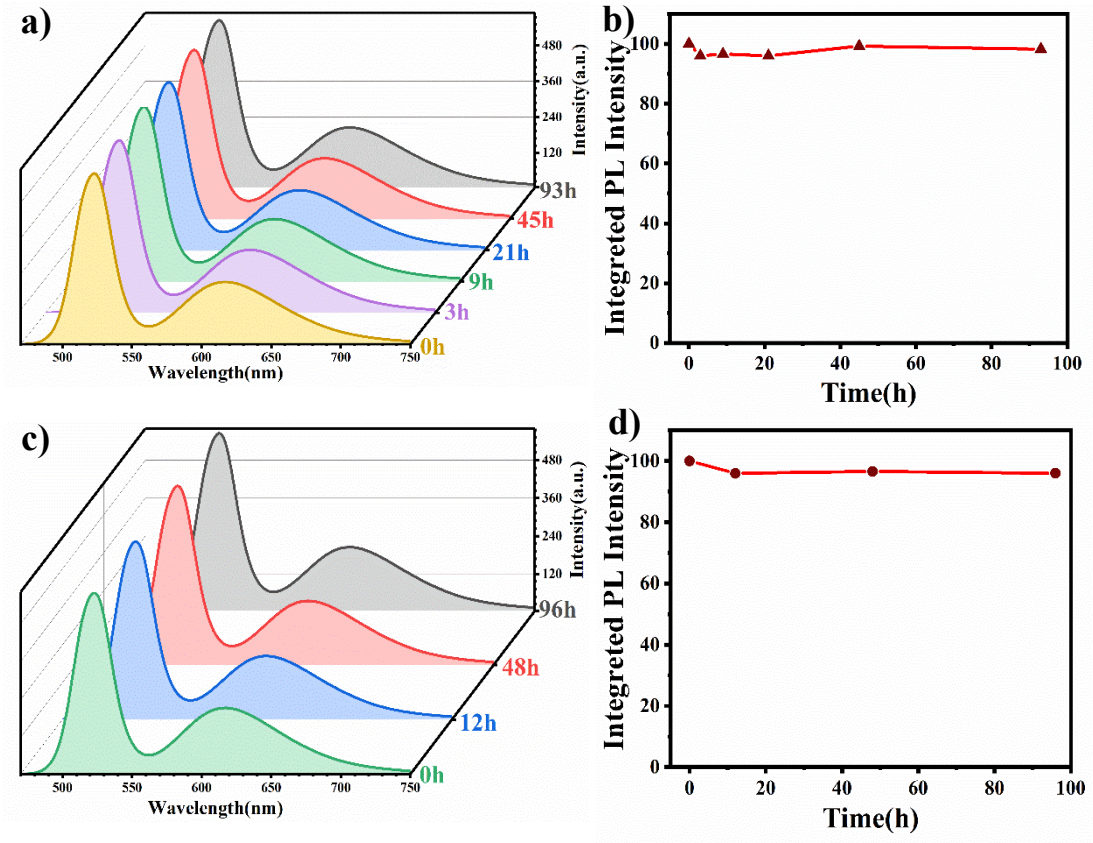

Fig. 7 (a) PL spectra (λ_{ex} = 450 nm) of QiG@glass under different duration blue light irradiation (b) Integrated photoluminescence intensities in light stability. (c) PL spectra (λ_{ex} = 450 nm) of QiG@glass under different duration oxygen conditions. (d) Integrated photoluminescence intensities in oxygen stability.

4. Conclusions

We successfully deposited $CsPbBr_3$ PQDs into borosilicate glass by melt quenching technique and heat treatment. The quantum efficiency PLQY of $CsPbBr_3$ reached 88.06% after the regulation of various components in the glass. QiG@glass film was prepared by scraping and coating technique. Tellurite glass with low melting point was double coated to protect the stability of phosphors. A red phosphor emitting a wide spectrum was used to improve the color rendering index. The color rendering index of single-luminescent center QiG@glass thin-film conversion W-LED device is up to 87.2, the corresponding color temperature is 3920K, and the color gamut of 111.92% of the NTSC standard.

Acknowledgement

Guoying Zhao acknowledges financial supported by Science and Technology Talents

Development Fund for Young Middle-aged Teachers Fund, Collaborative Innovation Fund (No. XTCX2022-03) of Shanghai Institute of Technology and Development of key technologies for the preparation and application of high-performance rare earth fluorescent block materials (No. BFXT-2022-D0046). Jingshan Hou acknowledges financial supported by the National Natural Science Foundation of China (No. 51902203). Yongzheng Fang acknowledges financial supported by the National Natural Science Foundation of China (No. 51472162).

References

[1] Cai C, Wang X, Ling L, et al. Photoluminescence enhancement in wide spectral range excitation in $CsPbBr_3$ nanocrystal/Ag nanostructure via surface plasmon coupling[J]. Optics Letters, 2019, 44(3): 658-661.

[2] Luo X, Lai R, Li Y, et al. Triplet energy transfer from $CsPbBr_3$ nanocrystals enabled by quantum confinement[J]. Journal of the American Chemical Society, 2019, 141(10): 4186-4190.

[3] Swarnkar A, Marshall A R, Sanehira E M, et al. Quantum dot–induced phase stabilization of α-$CsPbI_3$ perovskite for high-efficiency photovoltaics[J]. Science, 2016, 354(6308): 92-95.

[4] Yang B, Mei S, Zhu Y, et al. Precipitation promotion of highly emissive and stable $CsPbX_3$ (Cl, Br, I) perovskite quantum dots in borosilicate glass with alkaline earth modification[J]. Ceramics International, 2022.

[5] Li B, Zhang Y, Fu L, et al. Surface passivation engineering strategy to fully-inorganic cubic $CsPbI_3$ perovskites for high-performance solar cells[J]. Nature communications, 2018, 9(1): 1-8.

[6] Weng K, Long N, Guo Y, et al. Nanocrystallization of α-CsPbI3 perovskite nanocrystals in GeS_2-Sb_2S_3 based chalcogenide glass[J]. Journal of the European Ceramic Society, 2020, 40(12): 4148-4152.

[7] Yao J-S, Ge J, Han B-N, et al. Ce^{3+}-doping to modulate photoluminescence kinetics for efficient $CsPbBr_3$ nanocrystals based light-emitting diodes[J]. Journal of the American Chemical Society, 2018, 140(10): 3626-3634.

[8] Zhang Y, Zhang Z, Liu X, et al. A high quantum efficiency $CaAlSiN_3$: Eu^{2+} phosphor-in-glass with excellent optical performance for white light-emitting diodes and blue laser diodes[J]. Chemical Engineering Journal, 2020, 401: 125983.

[9] Yong Z-J, Guo S-Q, Ma J-P, et al. Doping-enhanced short-range order of perovskite nanocrystals

for near-unity violet luminescence quantum yield[J]. Journal of the American Chemical Society, 2018, 140(31): 9942-9951.

[10] Chen D, Liu Y, Yang C, et al. Promoting photoluminescence quantum yields of glass-stabilized $CsPbX_3$ (X= Cl, Br, I) perovskite quantum dots through fluorine doping[J]. Nanoscale, 2019, 11(37): 17216-17221.

[11] Cho J, Park J H, Kim J K, et al. White light□emitting diodes: history, progress, and future[J]. Laser & photonics reviews, 2017, 11(2): 1600147.

[12] Schubert E F, Kim J K. Solid-state light sources getting smart[J]. Science, 2005, 308(5726): 1274-1278.

[13] Tsao J Y, Crawford M H, Coltrin M E, et al. Toward smart and ultra□efficient solid□state lighting[J]. Advanced Optical Materials, 2014, 2(9): 809-836.

[14] Wierer Jr J J, Tsao J Y, Sizov D S. Comparison between blue lasers and light□emitting diodes for future solid□state lighting[J]. Laser & Photonics Reviews, 2013, 7(6): 963-993.

[15] Long X M, He J G, Zhou J, et al. A review on light-emitting diode based automotive headlamps[J]. Renewable & Sustainable Energy Reviews, 2015, 41: 29-41.

[16] Nair G B, Dhoble S J. A perspective perception on the applications of light-emitting diodes[J]. Luminescence, 2015, 30(8): 1167-1175.

[17] Appaiah P, Narendran N, Perera I U, et al. Effect of thermal stress and short-wavelength visible radiation on phosphor-embedded LED encapsulant degradation[J]. Optical Materials, 2015, 46: 6-11.

[18] Singh P, Tan C M. Time evolution of packaged LED lamp degradation in outdoor applications[J]. Optical Materials, 2018, 86: 148-154.

[19] Nam Y H, Han K, Chung W J, et al. Double encapsulation of $CsPbBr_3$ perovskite nanocrystals with inorganic glasses for robust color converters with wide color gamut[J]. ACS Applied Nano Materials, 2021, 4(7): 7072-7078.

[20] Zhu Y X, Yang B B, Lu Q, et al. Stable Dy-doped $CsPbBr_3$ quantum dot glass with enhanced optical performance[J]. Journal of Non-Crystalline Solids, 2022, 575.

[21] Chen H, Lin H, Xu J, et al. Chromaticity-tunable phosphor-in-glass for long-lifetime high-power warm w-LEDs[J]. Journal of Materials Chemistry C, 2015, 3(31): 8080-8089.

[22] Elkhoshkhany N, Essam R. Influence of La_2O_3 on the structural, optical and thermal properties of TeO_2–ZnO–Li_2O–Nb_2O_5 glass[J]. Journal of Non-Crystalline Solids, 2020, 536: 119994.

[23] Ataalla M, Afify A S, Hassan M, et al. Tungsten-based glasses for photochromic, electrochromic, gas sensors, and related applications: A review[J]. Journal of Non-Crystalline Solids, 2018, 491: 43-54.

[24] Guo Y, Liu X, Duan H, et al. Optimization by energy transfer process of 2.7 μm emission in highly Er^{3+}-doped tungsten-tellurite glasses[J]. Infrared Physics & Technology, 2019, 99: 49-54.

[25] Chen D, Xiang W, Liang X, et al. Advances in transparent glass–ceramic phosphors for white light-emitting diodes—A review[J]. Journal of the European Ceramic Society, 2015, 35(3): 859-869.

[26] Qi F, Shao X, Ma Y, et al. Improved luminescent performances of $CsPbI_3$ perovskite quantum dots via optimizing the proportion of boron-silicate glass and precipitation processing[J]. Opt Mater, 2022, 124: 111981.

[27] Yang B, Mei S, He H, et al. Lead oxide enables lead volatilization pollution inhibition and phase purity modulation in perovskite quantum dots embedded borosilicate glass[J]. Journal of the European Ceramic Society, 2022, 42(1): 258-265.

[28] Chen D, Yuan S, Chen J, et al. Robust $CsPbX_3$ (X= Cl, Br, and I) perovskite quantum dot embedded glasses: nanocrystallization, improved stability and visible full-spectral tunable emissions[J]. Journal of Materials Chemistry C, 2018, 6(47): 12864-12870.

[29] Xu Z, Liu X, Qiu J, et al. Enhanced luminescence of $CsPbBr_3$ perovskite quantum-dot-doped borosilicate glasses with Ag nanoparticles[J]. Optics Letters, 2019, 44(22): 5626-5629.

[30] Xu L, Zhao G, Meng S, et al. Enhanced luminescent performance for remote LEDs of Ce:YAG phosphor-in-glass film on regular textured glass substrate by using chemical wet-etching[J]. Ceram Int, 2018, 44: 22283-22288.

[31] Kim J S, Eswaran S K, Kwon O H, et al. Enhanced Luminescence Characteristics of Remote Yellow Silicate Phosphors Printed on Nanoscale Surface-Roughened Glass Substrates for White Light-Emitting Diodes[J]. Advanced Optical Materials, 2016, 4(7): 1081-1087.

[32] Kim S, Park H A, Bin Im W, et al. A low sintering temperature glass based on SiO_2-P_2O_5-ZnO-B_2O_3-R_2O system for white LEDs with high color rendering index[J]. Journal of the American Ceramic Society, 2017, 100(11): 5186-5192.

[33] Ahn S H, Nam Y H, Han K, et al. Phosphor-in-glass thick film formation with low sintering temperature phosphosilicate glass for robust white LED[J]. Journal of the American Ceramic Society, 2017, 100(4): 1280-1284.

[34] Han K, Lee S H, Choi Y G, et al. Improved color rendering index and thermal stability of white LEDs with phosphor-in-glass using the SiO_2-B_2O_3-ZnO-Na_2O glass system[J]. Journal of Non-Crystalline Solids, 2016, 445: 77-80.

[35] Hinostroza I E O, Desirena H, Hernandez J, et al. Eu^{3+}-doped glass as a color rendering index enhancer in phosphor-in-glass[J]. Journal of the American Ceramic Society, 2018, 101(7): 2914-2920.

[36] Huang P, Zhao Y Y, Wang J C, et al. Tunable chromaticity and high color rendering index of WLEDs with $CaAlSiN_3$:Eu^{2+} and YAG:Ce^{3+} dual phosphor-in-silica-glass[J]. Journal of the American Ceramic Society, 2020, 103(9): 4989-4998.

[37] Zhao Q C, Jiang G J, Wang Z M, et al. Chromaticity-tunable color converter of $CaAlSiN_3$:Eu^{2+} red phosphor film layer stacked YAG PiG for warm-WLED[J]. Journal of Materials Science-Materials in Electronics, 2018, 29(5): 4011-4019.

Preparation and Luminescent Performances of Tellurite Glass Coated $CsPbBr_3$@glass Film for Remote LED Color Converter

Huanhuan Zhang[1], Jialing Ou[1], Guoying Zhao[1*], Jingshan Hou[1], Yufeng Liu[1], Xin Qiao[2], Zhongzhi Wang[2], Ji-Guang Li[3], Yongzheng Fang[1*]

[1] *School of Materials Science and Engineering, Shanghai Institute of Technology, Shanghai 201418, PR China*

[2]*Baotou Research Institute of Rare Earths, Baotou, 014030, China*

[3]*Research Center for Functional Materials, National Institute for Materials Science, Tsukuba, Ibaraki 305-0044, Japan*

[*]*Corresponding author, E-mail addresses: zhaogy135@126.com; fyz1003@sina.com.*

ABSTRACT: We know that perovskite quantum dot (PQD) glass is one of the effective ways to achieve high stability, high reliability and high weather resistance. However, quantum dot glass is still unable to achieve completely uniform crystallization as a whole, so quantum dot glass has to be used in the form of powder by mixing glue. The use of organic matter leads to the problems of heat accumulation and stability. In this work, the concept of double cladding encapsulation was realized to solve the above problems in the application of quantum dot glass, and the remote inorganic fluorescent film is prepared. $CsPbBr_3$ PQDs embedded in borosilicate glass (PQDs@glass) were prepared using traditional melting-quenching and heat-treatment processes. By optimizing the raw material composition and melting conditions, excellent PQDs@glass were obtained, and its photoluminescence quantum yield (PLQY) was as high as 88.06%. The $CsPbBr_3$ PQDs embedded borosilicate glass has been dispersed in tellurite glass film again along with color-compensatory red-emitting nitride phosphor, which is a doubly encapsulated system with inorganic glass matrixes to improve stability and color-tunability. A series of prototypes light-emitting diode devices were assembled based on the as-made doubly encapsulated glass film with a commercial blue chip, resulting in bright white light luminescence at a color temperature of 3920 K and a high color rendering index of 87.2.

Keywords: Remote glass film; $CsPbBr_3$ perovskite quantum dot; High quantum yield; Double

Encapsulation

1. Introduction

Recently, due to the unique optical properties, inorganic cesium lead halide ($CsPbX_3$, X = Cl, Br, I) perovskite quantum dots (PQDs) have attracted growing attention[1-4]. The photoluminescence (PL) of lead halide perovskite PQDs covers the entire visible spectral region with high quantum yield, which may find potential applications in various photoelectronic devices[5-8]. Thermal corrosion of monodisperse perovskite $CsPbBr_3$ nanostructures in amorphous glass substrates and during co-sintering with low melting point glass is negligible, ensuring good luminous properties. By the passivation of surface traps in wet-chemical synthesis strategy, the photoluminescence quantum yields (PLQYs) of $CsPbBr_3$ can reach over 90% in green spectral region[9]. However, the PLQYs of glass-stabilized $CsPbBr_3$ is relatively lower than the colloidal counterpart, and the highest value of PLQY is 81% that is obtained from boron-germanium glass, which hampers their practical application for photoelectronic devices[10]. In general, borosilicate glass is characterized by excellent physical and chemical stability compared to other glass systems when exposed to air or moisture. Owning to the ligand sensibility of $CsPbBr_3$ PQDs in glass, it is necessary to optimize the borosilicate glass grid structure to achieve high PLQY and long-term stability.

As is known to all, the present commercial w-LED is assembled with yellow yttrium aluminum garnet phosphor and packaging material-organic epoxy silicone mixed, using "dispensing" technology means coated on LED chip[11-14]. However, as the LED power increases, the operating time increases, resulting in the PN junction temperature rise, at this time the chip temperature can be as high as 150~200 °C, which will make the phosphor temperature quenching effect[15,16]. It will also make LED device efficiency decline, color coordinate deviation, service life suddenly reduced service life of a sudden reduction[17,18]. It has been proposed to replace organic materials such as phosphorus in glass (PiG) with inorganic components. The PiG method is a simple mixture of transparent glass and phosphor sintered together at a certain temperature. Yoon et al. suggested a novel inorganic color converter for white LED with a single phosphor-in-glass (PiG) plate. $CsPbBr_3$ perovskite nanocrystals embedded in germanate glass was used as a green phosphor and mixed with a transparent silicate glass to prepare the PiG plate. The photo stability and thermal stability of $CsPbBr_3$ perovskite nanocrystals are improve[19]. Compared to glass ceramic plate, PiG film can be

easily sintered and its color coordination can be simply controlled by adjusting the rations of PQDs@glass and phosphors. In addition, PiG film has high thermal conductivity and adjustable high refractive index, which can diffuse the heat accumulated on the phosphorus layer onto the silicon glass substrate. Therefore, the PiG film exhibits the robust stability when compared with the organic encapsulants. Red nitride phosphors have been widely studied for their excellent photoluminescent behaviors. Unfortunately, the commercial red nitride phosphors suffer from the poor structural stability during the low temperature co-sintering procedure[20]. Therefore, the mother glass protecting the embedded phosphor particles is a key factor identifying the photoluminescent performances of PiG.

Tellurite glass is characterized by TeO_2 as the main component, often by adding some oxides and halides to improve the glass forming ability and stability[21]. As a kind of heavy metal oxide glasses, tellurite glass has its own unique advantages including: high refractive index (around 2.0), wide infrared transmission range (0.35-5 um), low phonon energy in oxide glass (about 600-850 cm^{-1}) and low melting temperature (800-950 °C)[22]. Benefiting from the high refractive index and low phonon energy, high absorption and emission cross section and low non-radiative transition rates of rare earth ion can be obtained[23,24]. As to the use of mother glass for PiG, the high refractive index of tellurite glass is favorable to matching the refractive index of doped phosphor to a greater extent[25]. Besides, the relatively low glass transition temperature will reduce the thermal corrosion of photoluminescent phase. Therefore, tellurite glass is considered to be an excellent candidate for PiG.

In this study, the concept of double cladding encapsulation was realized in borosilicate stabilized $CsPbBr_3$ PQDs using tellurite glass as the outer clad. Firstly, we obtain the $CsPbBr_3$ PQDs with the high quantum efficiency through the regulation of glass grid. By spinning coating technology, the as-made borosilicate stabilized $CsPbBr_3$ PQDs and commercial nitride phosphors are uniformly dispersed in tellurite glass on the silica substrate. Finally, after determining the optimal sintering temperature, we prepared a series of QiG(quantum dots in glass)@glass flakes and then mounted them on a blue chip with a wavelength of 450 nm to produce white light. The effects of sintering temperature and glass-phosphor ratio on the properties of QiG@glass were discussed.

2. Experimental section

2.1 Fabrication of $CsPbBr_3$ PQDs in borosilicate glasses

The glass carrier is prepared from high-purity SiO_2, H_3BO_3 and ZnO powders, and the perovskite components were added into Cs_2CO_3, $PbBr_2$ and KBr (CPB). The purity and supplier of all reagents are given in Table 2. All experiments are conducted without toxic and harmful organic reagents. All raw materials are first ground into a powder in an agate mortar and then transferred to a corundum crucible. The powder is melted in a muffle furnace at 1200 °C for 15 min. The molten glass is then poured into a preheated copper mold and immediately transferred to a muffle furnace at 350 °C and held for 2 h to release stress. Finally, the precursor glass was heat treated near the glass transition temperature to obtain $CsPbBr_3$ PQDs multi-component glass. Stored at a heat treatment temperature of 470 °C for 10 hours, a series of $CsPbBr_3$ PQDs multi-component glass samples were obtained. For further study, the resulting glass is ground into a powder or optically polished.

Table 1. Glass compositions [$xSiO_2$- (67-x) B_2O_3-16ZnO (x=35, 38, 41, 48, 58 mol%)] and the added perovskite-related components.

Sample	SiO_2	B_2O_3	ZnO	Cs_2CO_3	$PbBr_2$	KBr
35Si	35	32	16	9	3	6
38Si	38	29	16	9	3	6
41Si	41	26	16	9	3	6
48Si	48	19	16	9	3	6
58Si	58	9	16	9	3	6
8CPB	38	29	16	8	2	4
9CPB	38	29	16	9	3	6
10CPB	38	29	16	10	4	8
11CPB	38	29	16	11	5	10
12CPB	38	29	16	12	6	12
9CPB-1.8	38	29	16	9	5.4	10.8
9CPB-2.1	38	29	16	9	6.3	12.6
9CPB-2.4	38	29	16	9	7.2	14.4
9CPB-2.7	38	29	16	9	8.1	16.2
9CPB-3.0	38	29	16	9	9	18

2.2 Fabrication of QiG@glass films

Glasses with composition $20B_2O_3$-$60TeO_2$-10ZnO-$10Na_2O$ were prepared by using analytical grade B_2O_3, TeO_2, ZnO, Na_2CO_3 as starting materials. Based on a certain stoichiometric ratio, the starting materials were weighted and mixed together. It was thoroughly ground and placed in an

alumina crucible and then melted for 0.5 h at 950 °C in a muffle furnace. Subsequently, the melt were poured into a preheated brass mold and annealed at 300 °C for 15 h. Glass samples were cut and carefully polished to meet optical measurements. Each sample looks more transparent.

The slurries were mixed by suitable powder dosing: the prepared glass-stabilized $CsPbBr_3$ PQDs powder, $Sr_2Si_5N_8$ red phosphor, and tellurite glass matrix. All powders were mixed into organic vehicle which composition were terpilenol and ethyl cellulose at 80 K for 12 h by 700 rpm. The mixed slurry is spin coated onto the glass substrate (r_Φ = 20 mm) by scraping and then the resultant samples were dried at 150 °C for 5 h in order to make the organic matter completely volatile. Finally, QiG@glass film was obtained by sintering the glass film at 460 °C for 30 min.

Table 2. Purity and supplier of each starting reagent.

Start reagent	Purity	Supplier
SiO_2	GR	Shanghai Maclin Biochemical Technology Co., LTD
H_3BO_3	GR	Shanghai Titan Technology Co., LTD
ZnO	AR, 99.0%	Shanghai Titan Technology Co., LTD
Cs_2CO_3	99.9%	Shanghai Merrier Chemical Technology Co., LTD
KBr	AR, 99.0%	Sinopharm Chemical Reagent Co. LTD
$PbBr_2$	99 %	Shanghai Titan Technology Co., LTD
TeO_2	99.99%	Chengdu Zhongjian Materials Optoelectronic Materials Co., LTD
Na_2CO_3	AR, ≥ 99.8%	Shanghai Titan Technology Co., LTD

2.3 Characterization

The phase purity of phosphor powders and QiG@glass firms was confirmed by using an X-ray powder diffractometer (TD-3500, Dandong, China) with Cu Kα irradiation at 40 kV and 40 mA. The microstructure and elemental mappings were observed by a field-emission scanning microscope (SU70, Hitachi) equipped with an energy-dispersive X-ray spectroscope (EDS) system and Transmission Electron Microscopy (FEI Tecnai F20). The photo-luminescence (PL) and photo-luminescence excitation (PLE) of the samples were measured using a spectrometer (Hitachi F-7000) with a xenon discharge lamp. FS5 fluorescence spectrometer is standard equipped with absorption detector, which can achieve fluorescence and UV testing functions on the same instrument at the same time, so we tested the quantum yield by FS5. Decimal methods can also be applied to a wider

range of sample types and are the only reliable method for samples such as solid powder and thin films. The test requires an integrating sphere that is coupled to the fluorescence spectrometer as a test attachment. In absolute quantum yield testing, all light emitted by a sample is captured using an integrating sphere, and the quantum yield is determined by comparing the number of photons emitted to the number of photons absorbed. Such as formula (1):

$$\eta = \frac{number\ of\ photons\ emitted}{number\ of\ photons\ absorbed} \quad (1)$$

The difference in integral area between the sample and the reference indicates the number of the absorbed photons. The emitted photons were determined by integrating the related emission band. Test the blank curve with the blank sample that comes with the integrating sphere. The scattering curve and the sample curve are combined to calculate the quantum yield. The optical properties of the w-LED module are obtained in the integrating sphere, including chromaticity color coordinates, correlated color temperature (CCT), color rendering index (CRI), luminous efficiency, and electroluminescence (EL) emission spectroscopy (HAAS-2000).

3. Results and Discussion

3.1 Microstructure and luminescence of PQDs@glass

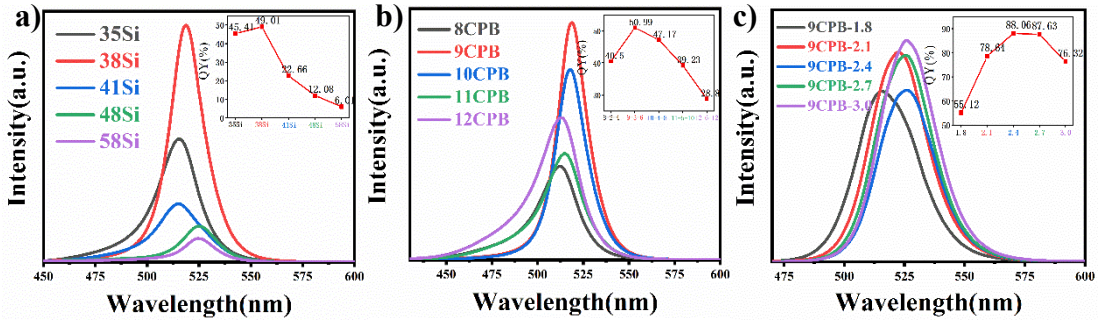

Fig. 1 (a-c) Photoluminescence spectra and PLQY of $xSiO_2$- (67-x) B_2O_3-16ZnO (x=35, 38, 41, 48, 58 mol%) glass with different CPB components excited at 365 nm.

Fig. 1 shows the photoluminescence (PL) spectra and PLQYs of $CsPbBr_3$ PQDs from borosilicate samples under excitation at 365 nm and 450 nm. It can be seen that the well crystallized $CsPbBr_3$ PQDs formed in B39Si28 glass containing 9CPB-2.4 has the highest PLQY value (88.06%). With the decrease of B/Si ratio, the emission intensity increases first and then decreases, reaching the maximum value at Si38B29, and the change of quantum yield also presents the similar trend. The photoluminescence of sample exhibits the narrow-band emission characteristics of

quantum dot materials. It can be seen from Fig. 1(a) that the luminescence of $CsPbBr_3$ PQDs doped glass is controlled by changing the topological structure of the glass. The glass grid structure has an important impact on the precipitation and growth of quantum dots from mother glass, which in turn affects the luminescence performance. Based on our previous work, there exists an optimal B/Si molar ratio that possesses the moderate glass rigidity, which can boost the precipitation of CPB elements and accelerate the growth of nanocrystals from glass network[26]. Therefore, Si38B29 sample is selected as glass host to optimize CPB concentration (PL spectra shown in Fig. 1(b and c))[27]. In order to compensate for the volatile loss of Br element during the melting procedure, excess amounts of halogen compounds, $PbBr_2$ and KBr, needed to be added to the raw material. With the increase of doped concentration, more and more quantum dots polymerize and grow in glass, resulting in an increase in PQDs concentration, it is worth noting that a moderate excess of Br supplementation in raw materials is more conducive to the growth of PQD in glass. The results show that the quantum efficiency of the sample reaches the maximum when the CPB concentration is further increased to $9Cs_2CO_3$−$7.2PbBr_2$−14.4KBr mol%.

As showed in TEM image (shown in Fig. 2(a)), the $CsPbBr_3$ PQDs are evenly dispersed in the glass matrix, and their average particle size is 2.98 nm. High-resolution TEM (HRTEM) image (Fig. 2(b)) evidences homogeneous precipitation of $CsPbBr_3$ PQDs with well-resolved lattice fringes with high-crystallinity, which shows clear lattice fringes with an interplanar distance of 0.288 nm. The lattice fringes have 0.288 nm interplanar distance that corresponds to the [200] lattice plane of the cubic $CsPbBr_3$[28,29]. It can be seen that the PQDs in the glass are different from the cubic form of the colloidal PQDs prepared by wet chemistry, and the PQDs in the glass is a spherical form, which may be due to the restriction effect of inorganic oxidized glass on the growth of PQDs. Elemental mapping of these nanocrystals suggested that these nanocrystals were highly rich in Cs, Pb and Br. In general, the precipitation of $CsPbBr_3$ nanocrystals in the sample was confirmed.

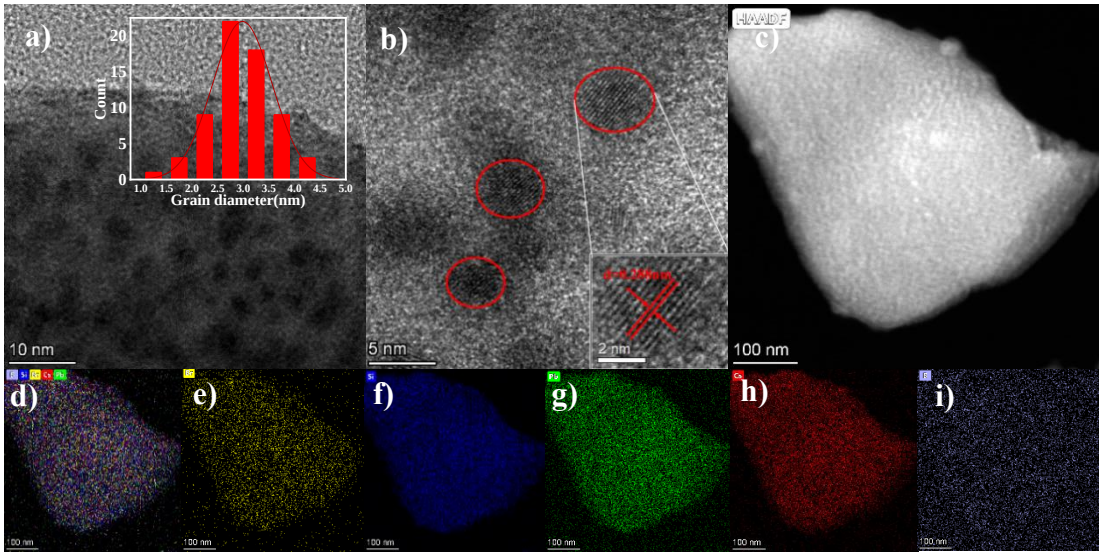

Fig. 2 (a and b) TEM image of the $CsPbBr_3$ PQDs@glass. (c) HRTEM micrograph of the $CsPbBr_3$ PQDs@glass. (d-i) B, Si, Cs, Pb, and Br elemental mappings.

3.2. Microstructure and luminescence of QiG@glass film.

QiG@glass films have high thermal stability compared to conventional organic encapsulation; Good moisture resistance; It has the characteristics of corrosion resistance and high chemical stability. The XRD patterns of quantum dot glass, red phosphor and QiG@glass samples are shown in Fig. 3(a). The different peaks correspond to the $Sr_2Si_5N_8$ and PQDs, which is in accord with that of the pure $Sr_2Si_5N_8$ phosphor and standard card of $CsPbBr_3$ (PDF #75–0412), respectively. The QiG@glass film has little effect on the phosphors, and the fluorescent crystal phase is intact in glass matrix. Furthermore, the 9CPB-2.4 QiG@glass film was chosen to check the possible reaction between as-prepared glass and the phosphor, SEM, EDS and EDS mapping were carried out. Fig. 3(b-h) indicates that the glass and phosphor powder are uniformly distributed in the tellurite glass matrix. The moderate concentration of pores in film is beneficial to reducing the reflection of incident light to improve the utility of pump light [30,31]. The cross section image (shown in Fig. 3(c)) suggests the phosphor layer with a thickness of approximately 24.54μm has been well adhered on the surface of silica glass substrate after sintering.

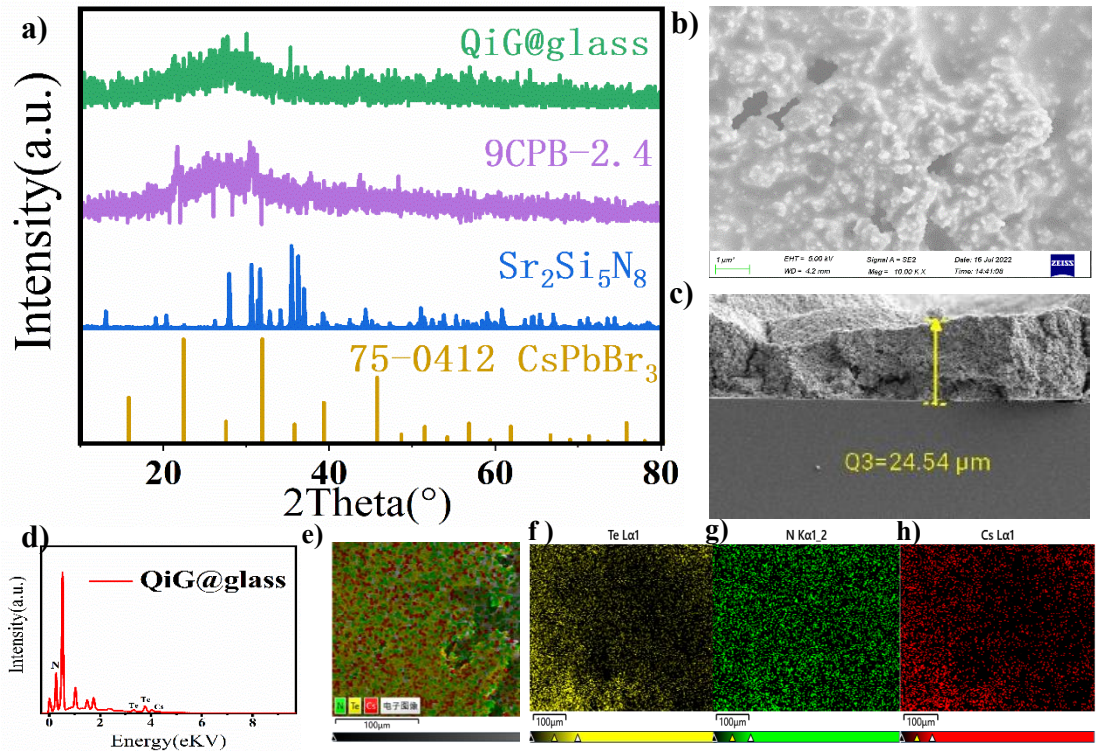

Fig. 3 (a) The XRD patterns of quantum dot glass, red phosphor and QiG@glass samples. (b and c) SEM of QiG@glass film. (d) EDS spectrum of QiG@glass film. (e-h) Mapping image of Te, N and Cs.

We prepared a series of W-LEDs by changing the ratio of quantum dot glass powder to red phosphor. To research the luminescence properties, the prepared QiG@glass film is assembled on the top of the blue chip under the 450 nm irradiation with a drive current of 10 mA (Fig. 4 (b)). To produce white light, we mixed the red phosphor $Sr_2Si_5N_8$ with glass powder at the content sub-point and then embedded in the tellurite glass to form a QiG@glass. The weight ratio of glass to phosphorus is adjusted from 10:1 to 14:1. The resulting electroluminescence diagram and color coordinates are shown in Fig. 4(a and c). According to EL spectrum and chromaticity diagram, the ratio of glass to phosphor is 13:1, which is the best ratio to produce white light. As the proportion of glass powder in QiG@glass increased, the 450 nm blue component in the spectrum increased, and the light color changed from warm white to cold white, as shown in Fig. 4(c).

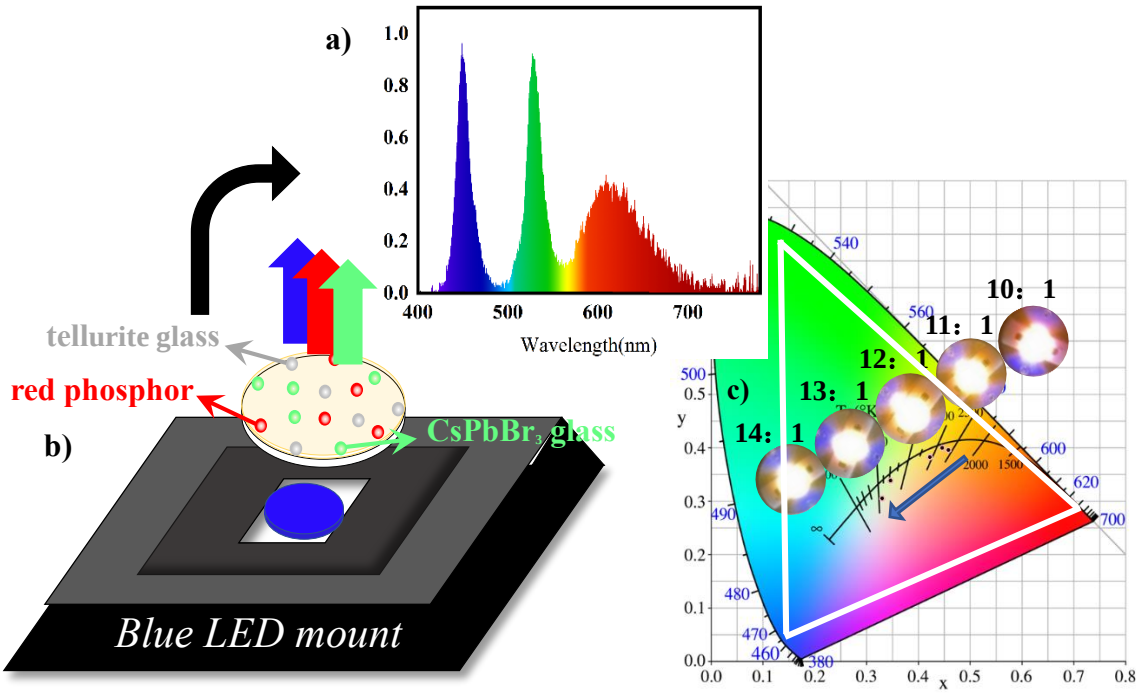

Fig. 4 (a) Optimum ratio electroluminescence diagram. (b) Schematic diagram of LED package. (c) Color coordinates at different scales and real pictures.

Fig. 5(a) shows the excitation and emission spectra of the glass powder and phosphor used in the experiment, respectively. It can be seen that the emission peak of the glass powder is located at 526 nm. It indicates that the emission spectrum of the glass powder and the excitation spectrum of the red powder have a large area of spectral overlap. The emission spectrum of glass powder can theoretically be reabsorbed by red powder and converted into red emission spectrum, which improves the emission intensity of red light, and correspondingly reduces the probability of green light transmitted out of the film to the space. QiG@glass films (the ratio of glass to red phosphor power was 13:1) were prepared at a sintering temperature of 460 °C to 490 °C. As the sintering temperature increased, the color of the sample gradually darkened, and the color rendering index decreased from 87.2 to 55.7. The color temperature increased from 3920 K to 12821 K. The results show that the sintering conditions of the QiG@glass film have a significant effect on the performance of the red phosphor. This may be due to the instability of the crystal phase structure of nitride in glass[32-37]. At a low sintering temperature of 460 °C, the thermal damage can be reduced for better luminous performance. At this temperature, warm white light with high visibility can be obtained.

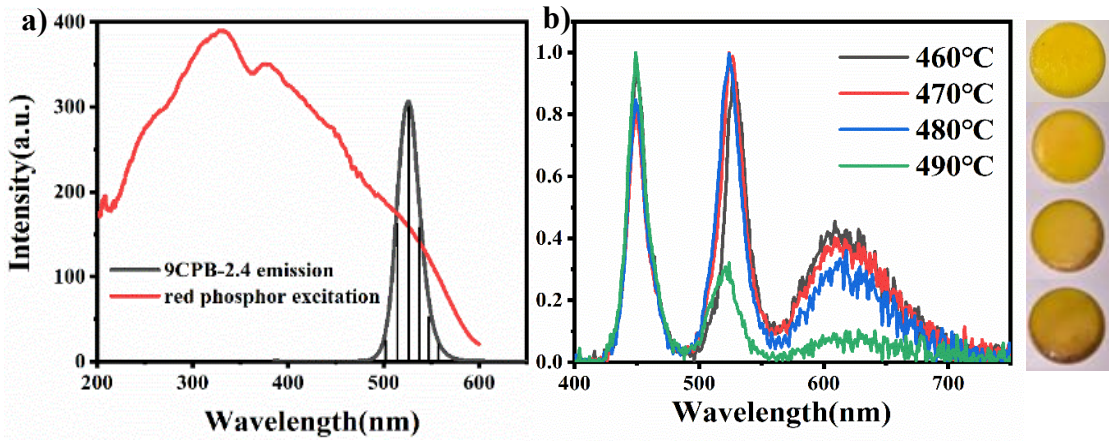

Fig. 5 (a) Emission spectrum of glass powder and excitation spectrum of phosphor powder. (b) The electroluminescence diagram of QiG@glass at different sintering temperatures.

3.3 The stability of QiG@glass film

The stability of QiG@glass is an important parameter for its applications. The PL temperature dependence was investigated (Fig. 6(a)), showing the PL spectra of QiG@glass at eight typical temperatures of 25, 50, 75, 100, 125, 150, 175 and 200 °C (298-473 K). With increasing of temperature (solid lines), the PL intensity decreased and its peak wavelength was blue-shifted. When the sample were cooled (dashed lines), the PL intensity and the shifted peak wavelength were reversibly recovered. These characteristic temperature dependent PL intensity change and emission peak shift have been commonly found in $CsPbBr_3$ perovskite nanocrystals, which can be attributed to the thermal expansion and phonon−electron interaction[19]. Furthermore, the long-term stability for the QiG@glass samples was investigated by dipping them in water. PL spectra shows that there is no obvious change of PL intensity (Fig. 6(c)) in water for 60 days. Under the protection of tellurite glass and borosilicate glass, the emission intensity is basically unchanged after 60 days of immersion in water. This result confirms that tellurite glass carriers and borosilicate glass are indeed effective in protecting PQDs from decomposition.

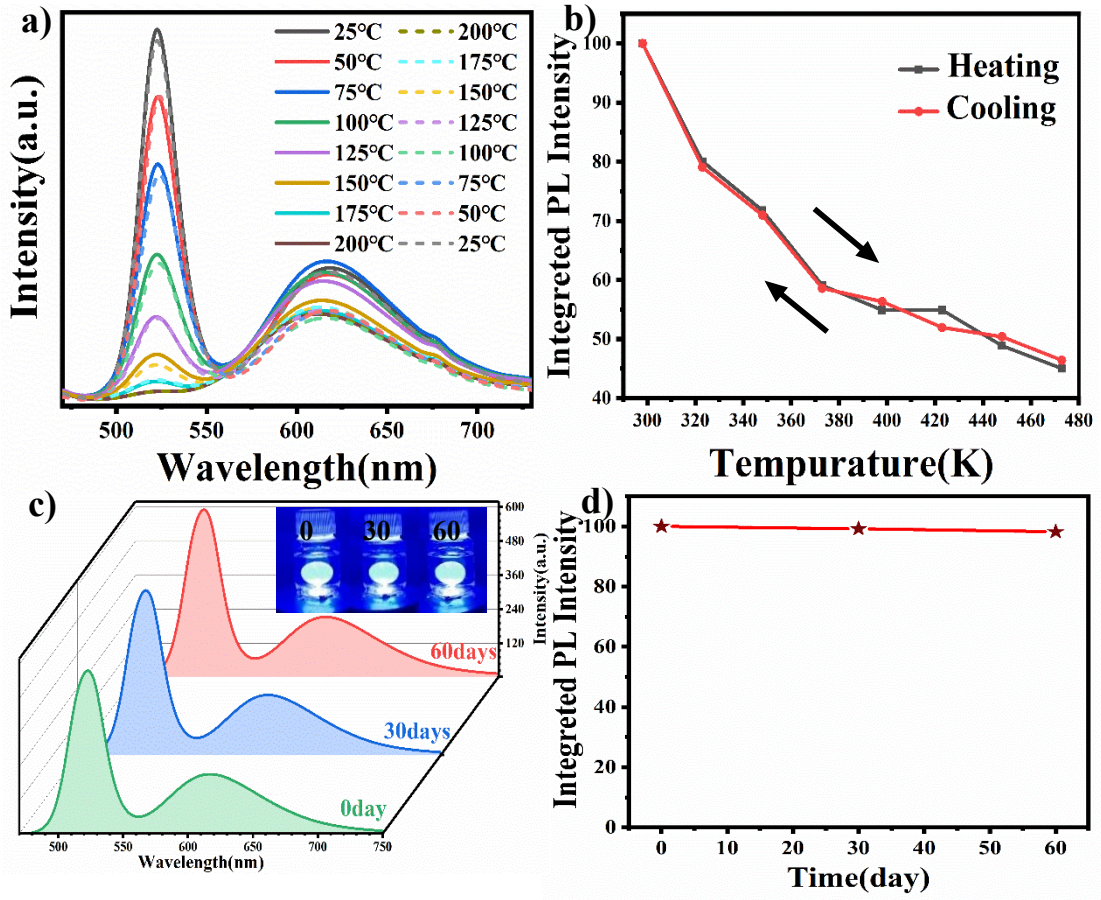

Fig. 6 (a) Temperature-dependent PL spectra (λ_{ex} = 450 nm) for the QiG@glass in the temperature range of 298-473 K. (b) Integral photoluminescence intensities of QiG@glass specimens recorded during thermal cycling experiment. (c) PL spectra for QiG@glass directly immersing in water for 60 days and inset is a photo of glass in water under the illumination of a blue light chip. (d) Integrated photoluminescence intensities in water stability.

The QIG@glass film was irradiated with a blue light of 300 mA forward current for 0, 3, 9, 21, 45, 93 h, equally its luminescence spectrum was tested (Fig. 7(a and b)), and the luminous intensity only decreased by about 3%. By introducing oxygen into the tube furnace, the oxygen stability of the film was studied by making the film stand in the oxygen environment for 0, 12, 48, 96 h. The luminescence spectrum shows (Fig. 7(c and d)) with no significant change in luminous intensity. Therefore, tellurite glass matrix can protect the stability of PQDs and phosphors effectively.

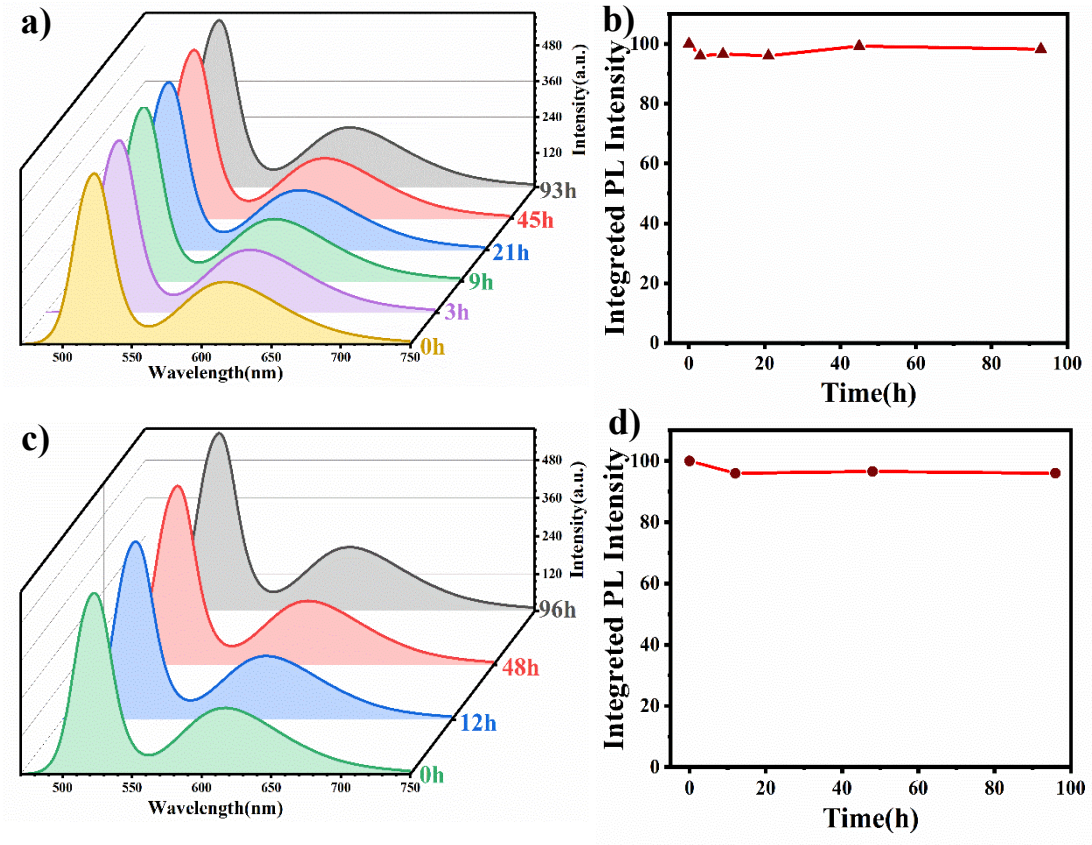

Fig. 7 (a) PL spectra (λ_{ex} = 450 nm) of QiG@glass under different duration blue light irradiation (b) Integrated photoluminescence intensities in light stability. (c) PL spectra (λ_{ex} = 450 nm) of QiG@glass under different duration oxygen conditions. (d) Integrated photoluminescence intensities in oxygen stability.

4. Conclusions

We successfully deposited $CsPbBr_3$ PQDs into borosilicate glass by melt quenching technique and heat treatment. The quantum efficiency PLQY of $CsPbBr_3$ reached 88.06% after the regulation of various components in the glass. QiG@glass film was prepared by scraping and coating technique. Tellurite glass with low melting point was double coated to protect the stability of phosphors. A red phosphor emitting a wide spectrum was used to improve the color rendering index. The color rendering index of single-luminescent center QiG@glass thin-film conversion W-LED device is up to 87.2, the corresponding color temperature is 3920K, and the color gamut of 111.92% of the NTSC standard.

Acknowledgement

Guoying Zhao acknowledges financial supported by Science and Technology Talents

Development Fund for Young Middle-aged Teachers Fund, Collaborative Innovation Fund (No. XTCX2022-03) of Shanghai Institute of Technology and Development of key technologies for the preparation and application of high-performance rare earth fluorescent block materials (No. BFXT-2022-D0046). Jingshan Hou acknowledges financial supported by the National Natural Science Foundation of China (No. 51902203). Yongzheng Fang acknowledges financial supported by the National Natural Science Foundation of China (No. 51472162).

References

[1] Cai C, Wang X, Ling L, et al. Photoluminescence enhancement in wide spectral range excitation in $CsPbBr_3$ nanocrystal/Ag nanostructure via surface plasmon coupling[J]. Optics Letters, 2019, 44(3): 658-661.

[2] Luo X, Lai R, Li Y, et al. Triplet energy transfer from $CsPbBr_3$ nanocrystals enabled by quantum confinement[J]. Journal of the American Chemical Society, 2019, 141(10): 4186-4190.

[3] Swarnkar A, Marshall A R, Sanehira E M, et al. Quantum dot–induced phase stabilization of α-$CsPbI_3$ perovskite for high-efficiency photovoltaics[J]. Science, 2016, 354(6308): 92-95.

[4] Yang B, Mei S, Zhu Y, et al. Precipitation promotion of highly emissive and stable $CsPbX_3$ (Cl, Br, I) perovskite quantum dots in borosilicate glass with alkaline earth modification[J]. Ceramics International, 2022.

[5] Li B, Zhang Y, Fu L, et al. Surface passivation engineering strategy to fully-inorganic cubic $CsPbI_3$ perovskites for high-performance solar cells[J]. Nature communications, 2018, 9(1): 1-8.

[6] Weng K, Long N, Guo Y, et al. Nanocrystallization of α-CsPbI3 perovskite nanocrystals in GeS_2-Sb_2S_3 based chalcogenide glass[J]. Journal of the European Ceramic Society, 2020, 40(12): 4148-4152.

[7] Yao J-S, Ge J, Han B-N, et al. Ce^{3+}-doping to modulate photoluminescence kinetics for efficient $CsPbBr_3$ nanocrystals based light-emitting diodes[J]. Journal of the American Chemical Society, 2018, 140(10): 3626-3634.

[8] Zhang Y, Zhang Z, Liu X, et al. A high quantum efficiency $CaAlSiN_3$: Eu^{2+} phosphor-in-glass with excellent optical performance for white light-emitting diodes and blue laser diodes[J]. Chemical Engineering Journal, 2020, 401: 125983.

[9] Yong Z-J, Guo S-Q, Ma J-P, et al. Doping-enhanced short-range order of perovskite nanocrystals

for near-unity violet luminescence quantum yield[J]. Journal of the American Chemical Society, 2018, 140(31): 9942-9951.

[10] Chen D, Liu Y, Yang C, et al. Promoting photoluminescence quantum yields of glass-stabilized $CsPbX_3$ (X= Cl, Br, I) perovskite quantum dots through fluorine doping[J]. Nanoscale, 2019, 11(37): 17216-17221.

[11] Cho J, Park J H, Kim J K, et al. White light□emitting diodes: history, progress, and future[J]. Laser & photonics reviews, 2017, 11(2): 1600147.

[12] Schubert E F, Kim J K. Solid-state light sources getting smart[J]. Science, 2005, 308(5726): 1274-1278.

[13] Tsao J Y, Crawford M H, Coltrin M E, et al. Toward smart and ultra□efficient solid□state lighting[J]. Advanced Optical Materials, 2014, 2(9): 809-836.

[14] Wierer Jr J J, Tsao J Y, Sizov D S. Comparison between blue lasers and light□emitting diodes for future solid□state lighting[J]. Laser & Photonics Reviews, 2013, 7(6): 963-993.

[15] Long X M, He J G, Zhou J, et al. A review on light-emitting diode based automotive headlamps[J]. Renewable & Sustainable Energy Reviews, 2015, 41: 29-41.

[16] Nair G B, Dhoble S J. A perspective perception on the applications of light-emitting diodes[J]. Luminescence, 2015, 30(8): 1167-1175.

[17] Appaiah P, Narendran N, Perera I U, et al. Effect of thermal stress and short-wavelength visible radiation on phosphor-embedded LED encapsulant degradation[J]. Optical Materials, 2015, 46: 6-11.

[18] Singh P, Tan C M. Time evolution of packaged LED lamp degradation in outdoor applications[J]. Optical Materials, 2018, 86: 148-154.

[19] Nam Y H, Han K, Chung W J, et al. Double encapsulation of $CsPbBr_3$ perovskite nanocrystals with inorganic glasses for robust color converters with wide color gamut[J]. ACS Applied Nano Materials, 2021, 4(7): 7072-7078.

[20] Zhu Y X, Yang B B, Lu Q, et al. Stable Dy-doped $CsPbBr_3$ quantum dot glass with enhanced optical performance[J]. Journal of Non-Crystalline Solids, 2022, 575.

[21] Chen H, Lin H, Xu J, et al. Chromaticity-tunable phosphor-in-glass for long-lifetime high-power warm w-LEDs[J]. Journal of Materials Chemistry C, 2015, 3(31): 8080-8089.

[22] Elkhoshkhany N, Essam R. Influence of La_2O_3 on the structural, optical and thermal properties of TeO_2–ZnO–Li_2O–Nb_2O_5 glass[J]. Journal of Non-Crystalline Solids, 2020, 536: 119994.

[23] Ataalla M, Afify A S, Hassan M, et al. Tungsten-based glasses for photochromic, electrochromic, gas sensors, and related applications: A review[J]. Journal of Non-Crystalline Solids, 2018, 491: 43-54.

[24] Guo Y, Liu X, Duan H, et al. Optimization by energy transfer process of 2.7 μm emission in highly Er^{3+}-doped tungsten-tellurite glasses[J]. Infrared Physics & Technology, 2019, 99: 49-54.

[25] Chen D, Xiang W, Liang X, et al. Advances in transparent glass–ceramic phosphors for white light-emitting diodes—A review[J]. Journal of the European Ceramic Society, 2015, 35(3): 859-869.

[26] Qi F, Shao X, Ma Y, et al. Improved luminescent performances of $CsPbI_3$ perovskite quantum dots via optimizing the proportion of boron-silicate glass and precipitation processing[J]. Opt Mater, 2022, 124: 111981.

[27] Yang B, Mei S, He H, et al. Lead oxide enables lead volatilization pollution inhibition and phase purity modulation in perovskite quantum dots embedded borosilicate glass[J]. Journal of the European Ceramic Society, 2022, 42(1): 258-265.

[28] Chen D, Yuan S, Chen J, et al. Robust $CsPbX_3$ (X= Cl, Br, and I) perovskite quantum dot embedded glasses: nanocrystallization, improved stability and visible full-spectral tunable emissions[J]. Journal of Materials Chemistry C, 2018, 6(47): 12864-12870.

[29] Xu Z, Liu X, Qiu J, et al. Enhanced luminescence of $CsPbBr_3$ perovskite quantum-dot-doped borosilicate glasses with Ag nanoparticles[J]. Optics Letters, 2019, 44(22): 5626-5629.

[30] Xu L, Zhao G, Meng S, et al. Enhanced luminescent performance for remote LEDs of Ce:YAG phosphor-in-glass film on regular textured glass substrate by using chemical wet-etching[J]. Ceram Int, 2018, 44: 22283-22288.

[31] Kim J S, Eswaran S K, Kwon O H, et al. Enhanced Luminescence Characteristics of Remote Yellow Silicate Phosphors Printed on Nanoscale Surface-Roughened Glass Substrates for White Light-Emitting Diodes[J]. Advanced Optical Materials, 2016, 4(7): 1081-1087.

[32] Kim S, Park H A, Bin Im W, et al. A low sintering temperature glass based on SiO_2-P_2O_5-ZnO-B_2O_3-R_2O system for white LEDs with high color rendering index[J]. Journal of the American Ceramic Society, 2017, 100(11): 5186-5192.

[33] Ahn S H, Nam Y H, Han K, et al. Phosphor-in-glass thick film formation with low sintering temperature phosphosilicate glass for robust white LED[J]. Journal of the American Ceramic Society, 2017, 100(4): 1280-1284.

[34] Han K, Lee S H, Choi Y G, et al. Improved color rendering index and thermal stability of white LEDs with phosphor-in-glass using the SiO_2-B_2O_3-ZnO-Na_2O glass system[J]. Journal of Non-Crystalline Solids, 2016, 445: 77-80.

[35] Hinostroza I E O, Desirena H, Hernandez J, et al. Eu^{3+}-doped glass as a color rendering index enhancer in phosphor-in-glass[J]. Journal of the American Ceramic Society, 2018, 101(7): 2914-2920.

[36] Huang P, Zhao Y Y, Wang J C, et al. Tunable chromaticity and high color rendering index of WLEDs with $CaAlSiN_3$:Eu^{2+} and YAG:Ce^{3+} dual phosphor-in-silica-glass[J]. Journal of the American Ceramic Society, 2020, 103(9): 4989-4998.

[37] Zhao Q C, Jiang G J, Wang Z M, et al. Chromaticity-tunable color converter of $CaAlSiN_3$:Eu^{2+} red phosphor film layer stacked YAG PiG for warm-WLED[J]. Journal of Materials Science-Materials in Electronics, 2018, 29(5): 4011-4019.

Conflict of Interest

No potential conflict of interest was reported by the authors.

CRediT authorship contribution statement

Huanhuan Zhang: Conceptualization, Writing - Original Draft, Investigation. **Jialing Ou:** Methodology, Data Curation, Investigation. **Guoying Zhao:** Methodology, Writing – Review & Editing. **Jingshan Hou:** Resources, Validation. **Yufeng Liu:** Resources, Formal analysis. **Xin Qiao:** Resources, Data curation. **Zhongzhi Wang:** Methodology, Resources. **JiGuang Li:** Resources. **Yongzheng Fang:** Funding acquisition, Supervision.